

# A Bayesian hierarchical model for methane emission source apportionment

William S. Daniels\*

Department of Applied Mathematics and Statistics,  
Colorado School of Mines

and

Douglas W. Nychka

Department of Applied Mathematics and Statistics,  
Colorado School of Mines

and

Dorit M. Hammerling

Department of Applied Mathematics and Statistics,  
Colorado School of Mines

## Abstract

Reducing methane emissions from the oil and gas sector is a key component of short-term climate action. Emission reduction efforts are often conducted at the individual site-level, where being able to apportion emissions between a finite number of potentially emitting equipment is necessary for leak detection and repair as well as regulatory reporting of annualized emissions. We present a hierarchical Bayesian model, referred to as the multisource detection, localization, and quantification (MDLQ) model, for performing source apportionment on oil and gas sites using methane measurements from point sensor networks. The MDLQ model accounts for autocorrelation in the sensor data and enforces sparsity in the emission rate estimates via a spike-and-slab prior, as oil and gas equipment often emit intermittently. We use the MDLQ model to apportion methane emissions on an experimental oil and gas site designed to release methane in known quantities, providing a means of model evaluation. Data from this experiment are unique in their size (i.e., the number of controlled releases) and in their close approximation of emission characteristics on real oil and gas sites. As such, this study provides a baseline level of apportionment accuracy that can be expected when using point sensor networks on operational sites.

*Keywords:* climate change, oil and gas emissions, Bayesian inverse modeling, Gibbs sampling, spike-and-slab prior

---

\*wdaniels@mines.edu

# 1 Introduction

By 2050, climate change is projected to cause an additional 14.5 million deaths and \$12.5 trillion in economic losses worldwide due to an increase in the frequency and severity of extreme weather events (World Economic Forum 2024). Rising concentrations of carbon dioxide and methane in the atmosphere are the primary drivers of climate change, making it crucial to reduce emissions of these gasses. Methane, in particular, provides an important opportunity to mitigate the near-term impacts of climate change given its relatively short lifetime in the atmosphere and high heat trapping potential compared to carbon dioxide (Szopa et al. 2021).

The oil and gas industry accounts for 22% of global anthropogenic methane emissions (O'Rourke et al. 2021, Crippa et al. 2021) and is a viable opportunity for emissions reductions given that: 1) emissions from equipment malfunctions can often be mitigated quickly once they are identified, and 2) technological improvements and facility design innovations can eliminate emissions from normally operating equipment such as pneumatic controllers (Nisbet et al. 2020). Knowing which pieces of equipment are emitting and their emission rates at any given time is necessary to both prioritize mitigation efforts and verify that long term emission reduction strategies are working. However, estimating emission source and rate based on ambient methane measurements is a challenging inverse problem due to the turbulent nature of near-field atmospheric transport, the degree of variability in emission rates, and the fact that only a subset of oil and gas equipment are emitting at a given time.

In this article, we analyze in situ sensor data from an experimental oil and gas site where methane is released at known rates in a way that emulates real-world emission characteristics. This site is called the Methane Emissions Technology Evaluation Center (METEC). Sensor data collected at METEC come as close as possible to data from a real

oil and gas site while still knowing ground truth emission source and rate. We develop a Bayesian hierarchical model for performing methane emission source apportionment at METEC, and by extension, on real oil and gas sites. We call this model the multisource detection, localization, and quantification (MDLQ) model. The MDLQ model combines an atmospheric transport model with a multivariate time series model for the sensor data. This is the first study, to our knowledge, that pairs a novel inversion method with a controlled release experiment that is sufficiently realistic to generalize to operating oil and gas sites.

## 1.1 Methane releases at METEC

The METEC facility, shown in Figure 1, is instrumented with real oil and gas equipment, such as wellheads and separators, but does not actually produce oil or gas. Instead, known quantities of methane are released from typical leak points on the oil and gas equipment. The controlled releases at METEC emulate the following characteristics of methane emissions on active oil and gas sites: emissions can last from minutes to days with rates that vary over time, any subset of the equipment can emit simultaneously, and there can be periods of no emissions (Cusworth et al. 2021, Wang et al. 2022, Daniels et al. 2023).

The METEC experiment consists of 337 releases conducted from February 5 to April 30, 2024. Releases are separated by periods of no emissions, and each release consists of emissions from a subset of the five equipment groups shown in Figure 1. These experiments provide a significantly larger and more realistic sample of methane emissions than other site-level inversion studies in the literature. For example, Cartwright et al. (2019) analyze two releases, Newman et al. (2024) analyze three releases, and Kumar et al. (2022) analyze 26 releases. The ability to apportion methane emissions using a small number of sensors is influenced by site layout, wind, and other meteorological conditions, making it important

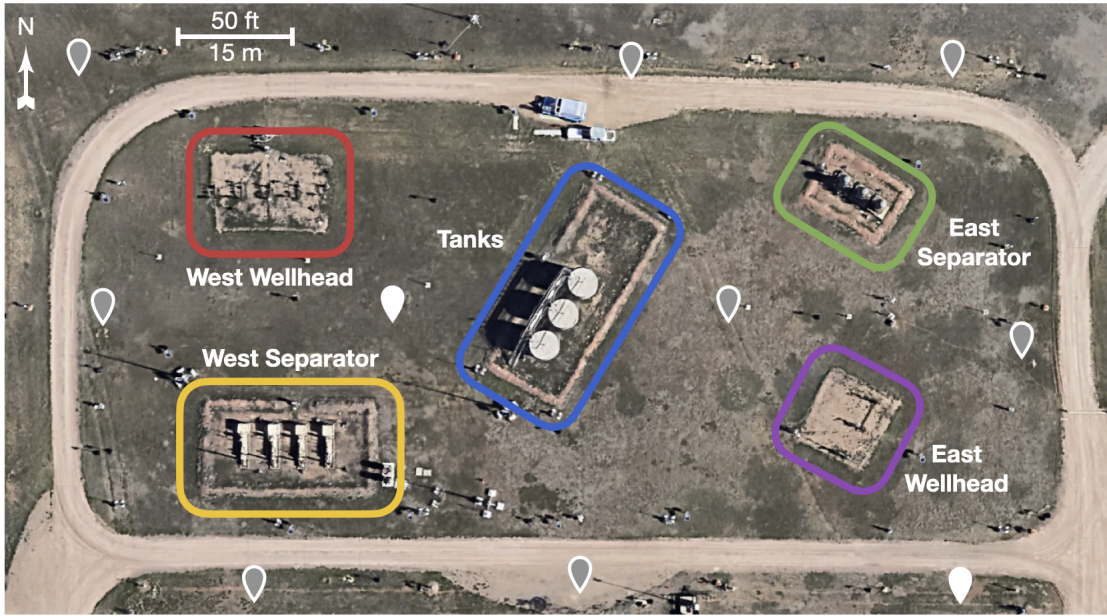


Figure 1: Aerial view of the METEC facility located in Fort Collins, Colorado. The five potential emission sources are identified with colored squares, and the locations of the 10 methane sensors are marked with pins. Pins with a gray interior show sensors that measure wind speed and direction in addition to methane concentrations.

to assess the performance of a statistical inversion over a wide range of conditions.

Furthermore, the releases in this study better emulate the emission characteristics of active oil and gas sites than similar studies in the literature. For example, Weidmann et al. (2022) evaluate their method on methane releases with known start and end times, and Hirst et al. (2020) perform releases in flat empty locations with simple atmospheric transport. As such, the modeling results in this study are more likely to generalize to real oil and gas sites of similar size and complexity to METEC and provide a baseline level of apportionment accuracy on these sites.

## 1.2 The continuous monitoring inverse problem

The MDLQ model uses methane concentration measurements from a network of in situ sensors placed directly on oil and gas sites to apportion emissions. We refer to this type of sensor system as a continuous monitoring system (CMS). The locations of the CMS sensors

in this study are shown as pins in Figure 1. Each sensor measures ambient methane concentrations once per second, which are averaged in situ every minute. Let  $\mathbf{y} \equiv \{y_1, \dots, y_n\}$  denote the minute-frequency CMS concentration measurements, where  $n$  is determined by the amount of time over which the inversion is to be taken (discussed further in Section 3.3). As with most remote sensing technologies, an atmospheric inversion is required to translate  $\mathbf{y}$  into estimates of emission source and rate.

Many of the existing inversion techniques for CMS rely on the assumption that one source is emitting at a time (Xue et al. 2017, Cartwright et al. 2019, Kumar et al. 2022, Daniels et al. 2024a), which is a known simplification of real emission characteristics (Wang et al. 2022, Kunkel et al. 2023). Inversion techniques that allow for multiple simultaneous emission sources often assume that the CMS concentration measurements are a linear combination of concentration predictions from an atmospheric transport model,

$$\mathbf{y} = X\boldsymbol{\beta} + \boldsymbol{\epsilon}, \tag{1}$$

where emission rates for the  $p$  potential sources on the site,  $\boldsymbol{\beta} \equiv \{\beta_1, \dots, \beta_p\}$ , are assumed to be constant within the temporal extent of the inversion. The design matrix is often constructed as  $X \equiv [\mathbf{x}^{(1)} \dots \mathbf{x}^{(p)}] \in \mathbb{R}^{n \times p}$ , where each  $\mathbf{x}^{(i)} \in \mathbb{R}^n$  for  $i = \{1, \dots, p\}$  contain the concentration predictions from the transport model at all sensor locations assuming that source  $i$  is emitting at a unitary rate. In many studies, the errors  $\boldsymbol{\epsilon} \equiv \{\epsilon_1, \dots, \epsilon_n\}$  are assumed normal, independent, and identically distributed (Ars et al. 2017, Cartwright et al. 2019, Hirst et al. 2020, Newman et al. 2024), which is another limitation given that  $\mathbf{y}$  are time series data. In this study, we are primarily concerned with estimates for  $\boldsymbol{\beta}$ , as these tell us the subset of sources that are emitting and their rate.

Our approach, implemented in the MDLQ model, assumes the same linear model as Equation 1 at the data level, but further models  $\boldsymbol{\beta}$  as a mixture distribution with a point

mass at 0 kg/hr. This process model allows for rate estimates to be identically zero, a necessary property given that potential sources are often not emitting. We use a Dirac delta function to implement the point-mass, providing an extension to the methodology in Weidmann et al. (2022), who used a narrow Gaussian to approximate the point mass. This extension eliminates the need to tune the relative widths of the components of the mixture distribution. Finally, following Ganesan et al. (2014), we allow  $\epsilon$  to be autocorrelated since the elements of  $\mathbf{y}$  are observed over time at 1-minute intervals. We extend the methods in Ganesan et al. (2014) by parameterizing the covariance matrix such that the determinant and inverse have closed forms, allowing for fast computation.

### 1.3 Outline

In Section 2, we provide additional details about the METEC experiment, atmospheric transport model, and our background-removal procedure. In Section 3, we present the MDLQ model and our procedure for running it operationally, rather than on experiments with known start and end times. In Section 4, we present source apportionment results for the METEC experiment, probe the limitations of the MDLQ model via a simulation study, and compare our results to current state-of-the-art methods from the literature.

## 2 Data

### 2.1 METEC controlled release and measurement data

Methane concentration data for the METEC experiment come from a network of 10 CMS sensors installed around the facility at a height of 2 m. Eight of the sensors are also equipped with an anemometer to measure wind speed and direction in the horizontal plane. Wind

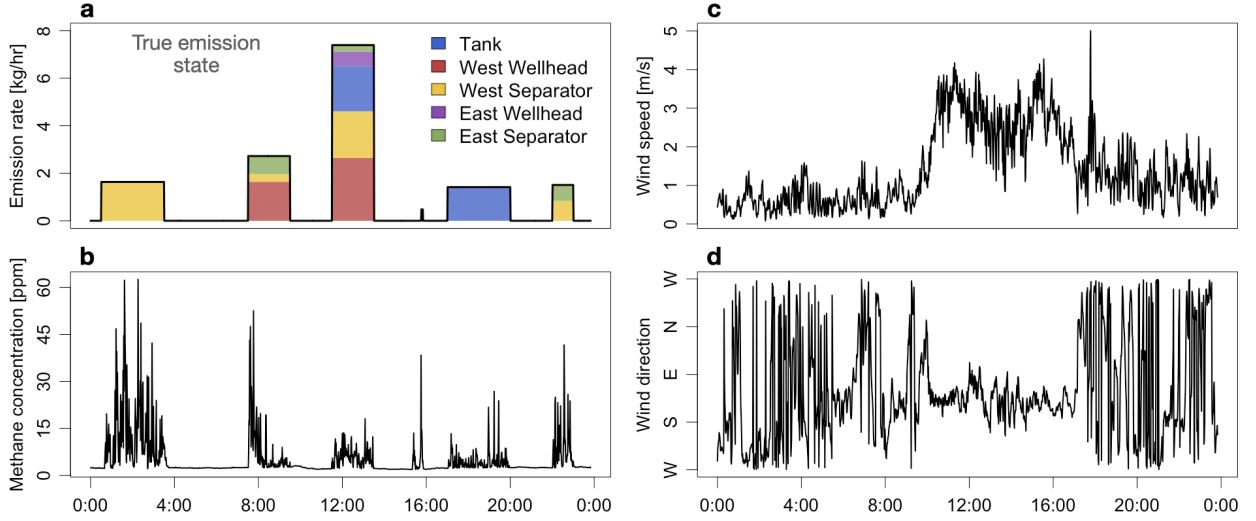


Figure 2: *Example data from February 12, 2024. (a) True release data, with color corresponding to the emission source. (b) Minute-by-minute maximum of the concentration observations across the 10 CMS sensors. (c) Minute-by-minute median of the wind speed observations across the 8 sensors with anemometers. (d) Minute-by-minute circular median of the wind direction observations across the 8 sensors with anemometers.*

data are necessary to forward simulate the transport of methane from the emission sources to the sensor locations (discussed further in Section 2.2). The properties (e.g., accuracy and precision) of the CMS sensors in this study are comparable to the sensors being used operationally to mitigate emissions. Full sensor specifications are provided in Section S1 of the Supporting Information (SI) file.

Unlike many studies in the literature, the controlled releases in this experiment were performed around-the-clock to evaluate the model under both daytime and nighttime meteorology. Each release consists of emissions from a subset of the five potential emission sources shown in Figure 1. Emission rates were constant within a given release, but could be different between the emitting equipment. Across the 337 releases, equipment-level release rates ranged from 0.08 to 7.2 kg/hr, emission durations ranged from 1.1 minutes to 8.0 hours, and release heights ranged from 0.12 m to 5.5 m.

As an example, Figure 2 shows the true emission state during a 24-hour period and the corresponding concentration and wind data from the CMS sensors. In Figure 2(b), we

plot the minute-by-minute maximum concentration observation across the 10 CMS sensors as a condensed summary of the data. Figure S4 in the SI shows the methane concentration measurements from all 10 CMS sensors separately. Notice that the concentration enhancements align with the timing of the controlled releases, but the amplitude of the enhancements do not follow the magnitude of the releases. This is because the sensors are not located at the release points, and meteorological effects such as wind speed affect the transport of methane and the resulting concentrations at the sensor locations. Modeling this transport is critical for an accurate inversion of emission source and rate.

## 2.2 Atmospheric transport model

We use a Gaussian puff model (GPM) to simulate the transport of methane from the emission sources to the sensor locations. The GPM approximates a continuous release of methane by simulating the movement of many small “puffs” of methane that are modeled as 3-dimensional Gaussian-like distributions. Discretizing a continuous release of methane in this manner allows the GPM to move each puff according to the wind conditions at its location in both space and time, providing a more accurate representation of atmospheric transport than models that assume steady state conditions. Note that the GPM treats methane as a passive tracer in the atmosphere, which is a reasonable assumption at the time and distance scales used for source apportionment on oil and gas sites. We describe the GPM below, but see Jia et al. (2025) or Stockie (2011) for more details.

Consider a coordinate system in which emission source  $i$  is located at  $(0, 0, H_i)$ . The puffs of methane from this source will all originate at this point. New puffs are created at a given frequency,  $\delta t$ , by default once per second, and the coordinates are rotated for each puff so that the positive  $x$ -direction is pointed in the downwind direction at the time



of puff creation. In this coordinate system, the predicted methane concentration at sensor location  $(x, y, z)$  from a given puff, index by  $j$ , that originated at  $(0, 0, H_i)$  and has been in existence for time  $t$  is modeled as

$$c_j^{(i)}(x, y, z, t) = \frac{Q}{(2\pi)^{3/2}\sigma_y^2\sigma_z} \exp\left(-\frac{(x-ut)^2 + y^2}{2\sigma_y^2}\right) \left[ \exp\left(-\frac{(z-H_i)^2}{2\sigma_z^2}\right) + \exp\left(-\frac{(z+H_i)^2}{2\sigma_z^2}\right) \right],$$

where  $Q$  is the mass of methane contained in puff  $j$ ,  $\sigma_y$  and  $\sigma_z$  are the dispersion parameters in the  $y$  and  $z$  directions, respectively, and  $u$  is the wind speed at the time of puff creation. The value of  $Q$  is a function of the specified emission rate,  $q$ , and the puff creation frequency,  $\delta t$ . The GPM requires time,  $t$ , to be discretized at a fixed multiple of the puff creation frequency,  $\delta t$ .

At each subsequent time step, a new puff is created at  $(0, 0, H_i)$  and puffs already in existence are transported based on the wind speed and direction from their respective creation times. The GPM used in this study assumes zero advection in the vertical direction, as wind data in this dimension are hard to obtain in practice, but the puffs do grow more diffuse in all three physical dimension as they move downwind. The total methane concentration at sensor location  $(x, y, z)$  and time  $t$  from source  $i$  is then

$$c^{(i)}(x, y, z, t) = \sum_{j=1}^P c_j^{(i)}(x, y, z, t),$$

where  $P$  is the number of puffs in existence at time  $t$ .

The dispersion parameters  $\sigma_y$  and  $\sigma_z$  control the size of each puff as it moves downwind and becomes more diffuse over time. We specify  $\sigma_y$  and  $\sigma_z$  using the EPA parameterization of the Pasquill-Gifford-Turner dispersion scheme (Pasquill 1961, Turner 1970, EPA 1992). Under this parameterization, both  $\sigma_y$  and  $\sigma_z$  are functions of stability class and

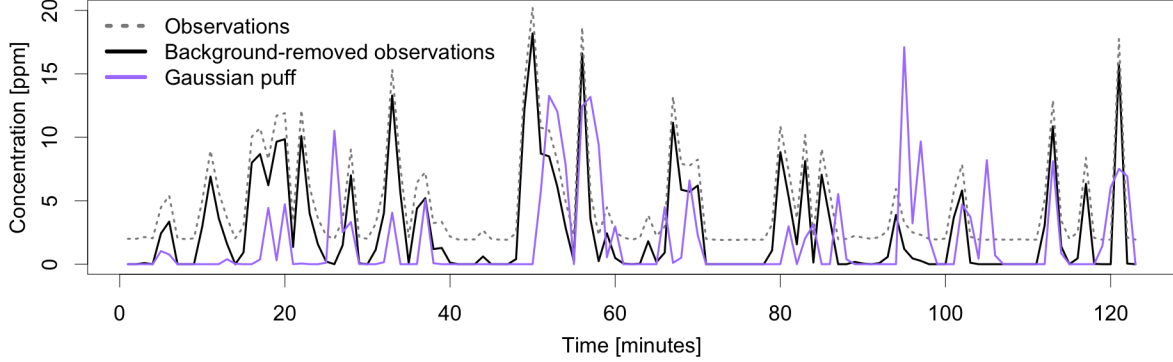


Figure 3: *Methane concentration observations and concentration predictions from the Gaussian puff atmospheric dispersion model during one of the METEC controlled releases.*

monotonically increase with total distance traveled (see Section S2 in the SI for details).

As an example, Figure 3 shows concentration observations from one of the CMS sensors during a controlled release and the corresponding output from the GPM scaled by the true release rate. Background-removed concentration observations are also included in this figure, which we discuss next in Section 2.3.

## 2.3 Background estimation and removal

Background methane concentrations are always present in the atmosphere but are not modeled by the GPM. We must therefore estimate the methane background and remove it from the CMS observations before evaluating model-data mismatch, as failing to do so would introduce upward bias in the emission rate estimates from the MDLQ.

Hirst et al. (2020) include background concentrations as a parameter to be determined in their inversion model. However, we find that the methane background can be accurately estimated before running an inversion by using the gradient-based spike detection algorithm from Daniels et al. (2024a). This algorithm identifies sharply elevated concentration observations (“spikes”) in the CMS data and estimates a local background for each as an average of the concentration observations immediately preceding and following the spike.

Figure 3 shows the raw concentration observations from one of the CMS sensors and the background-corrected concentrations using this algorithm.

This method for estimating the methane background imposes no assumptions about its spatial or temporal homogeneity nor does it require fitting a spatiotemporal model. Furthermore, we have found that estimating the background using a fixed value, such as the 5<sup>th</sup> percentile from Cartwright et al. (2019), often underestimates the true background by a few parts per million. This can lead to large errors in the inferred emission rates when the amplitude of the concentration enhancements is on a similar scale as the errors in the background estimate.

## 3 Model

### 3.1 Bayesian hierarchical model

There are three layers to the MDLQ model, which are summarized in Figure 4. The data layer (highest layer) contains a model for the CMS concentration observations. The process layer (middle layer) contains a model for the latent methane emission process that we do not directly observe. Finally, the parameter layer (lowest layer) contains priors for the model parameters that are not of direct interest for methane emission source apportionment but still contain important uncertainty information.

#### 3.1.1 Data layer

Our model for the CMS concentration data takes the form of a multiple linear regression,

$$\mathbf{y} = X\boldsymbol{\beta} + \boldsymbol{\epsilon},$$

where  $\mathbf{y} \equiv \{y_1, \dots, y_n\}$  are the background-corrected CMS concentration observations at a

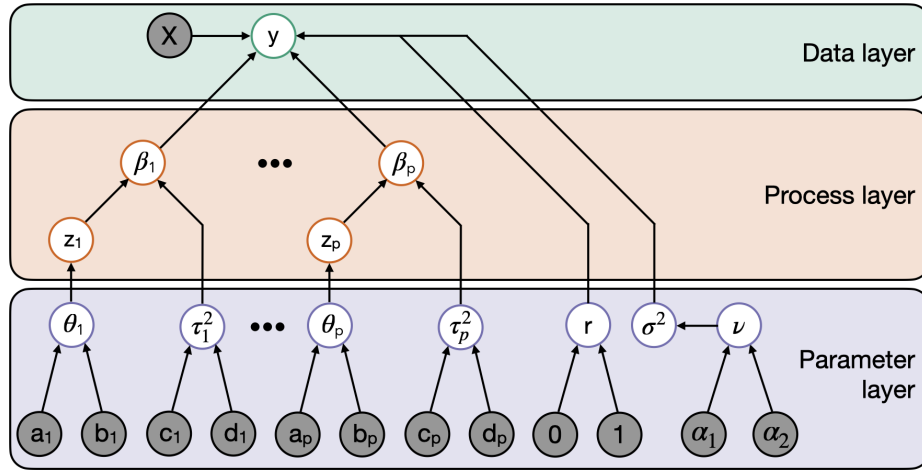


Figure 4: *Hierarchical structure and conditional independencies of the MDLQ model. Each circle represents a parameter, with fixed hyperparameters in gray and random variables in white. Arrows indicate when one parameter is a function of other parameters.*

1-minute frequency. We “stack” the concentration observations from all 10 CMS sensors in  $\mathbf{y}$ , as we want to leverage the information provided by each sensor jointly when performing the inversion, rather than performing a separate inversion for each sensor. The length of  $\mathbf{y}$  will reflect the choice of inversion length (discussed in Section 3.3), as  $n$  is equal to the number of 1-minute time steps used in the inversion multiplied by the number of sensors. We define the design matrix as  $X \equiv [\mathbf{x}^{(1)} \dots \mathbf{x}^{(p)}] \in \mathbb{R}^{n \times p}$ , where each  $\mathbf{x}^{(i)} \in \mathbb{R}^n$  for  $i = \{1, \dots, p\}$  denotes the concentration predictions from the GPM at all 10 CMS sensor locations assuming that source  $i$  is emitting at a unitary emission rate. We again “stack” the predicted concentrations at all sensor locations in  $\mathbf{x}^{(i)}$  to match the form of  $\mathbf{y}$ . Using the notation from Section 2.2, each  $\mathbf{x}^{(i)} = [c^{(i)}(x_1, y_1, z_1, t \in T), \dots, c^{(i)}(x_{10}, y_{10}, z_{10}, t \in T)]$ , where  $x_k$ ,  $y_k$ , and  $z_k$  are the spatial location of the  $k^{\text{th}}$  sensor,  $T$  is the temporal domain of the inversion, and  $c(\cdot)$  are the concentration predictions assuming that source  $i$  is emitting. Finally,  $\boldsymbol{\beta} \equiv \{\beta_1, \dots, \beta_p\}$  are the emission rates for the  $p$  sources on the site, which are assumed to be constant within the temporal extent of the inversion.

We assume that the errors  $\boldsymbol{\epsilon} \equiv \{\epsilon_1, \dots, \epsilon_n\}$  follow a multivariate normal, such that

$\epsilon \sim N(0, \sigma^2 R)$ , where  $R \in \mathbb{R}^{n \times n}$  contains the correlation structure of an AR(1) process and is solely a function of a correlation parameter  $r \in [0, 1]$ . The exact form of  $R$  is given in Section S10 of the SI. Modeling autocorrelation in  $\epsilon$  extends previous work and results in better coverage of the credible intervals (see Section S8 in the SI for details). The order of the autocorrelation model was selected through a visual analysis of partial autocorrelation functions; we find that an AR(1) often captures most of the autocorrelation in  $\epsilon$ . Additionally, using an AR(1) results in a covariance matrix with closed forms for both the inverse and determinant (Bodin et al. 2012), which allow for efficient sampling.

### 3.1.2 Process layer

The methane emission rate for each source takes the form of a mixture model with a point mass at 0 kg/hr, given by

$$\beta_i \sim \begin{cases} 0 & z_i = 0 \\ \text{Exp}(\tau_i^2 \sigma^2) & z_i = 1, \end{cases}$$

where the indicator  $z_i \in \{0, 1\}$  is modeled as  $z_i \sim \text{Bernoulli}(\theta_i)$ . This model is an example of a sparsity enforcing spike-and-slab prior (Mitchell & Beauchamp 1988). Sparsity in the emission rates is an intentional property of the MDLQ model, as potential emission sources on oil and gas sites are often not emitting. Previous work has found that emission rates over time follow a right skewed distribution (Daniels et al. 2023), so we use an exponential for the non-zero component of the mixture parameterized with a scale parameter given by  $\tau_i^2 \sigma^2$ . This scale parameter allows the exponential to scale with the magnitude of  $\mathbf{y}$ , making it easier to interpret MDLQ parameter estimates in other applications where  $\mathbf{y}$  might have a very different magnitude. Furthermore, the exponential component forces  $\beta$  to have non-negative support, as there are no methane sinks on oil and gas sites.

This variant of the spike-and-slab prior uses a discrete point-mass as the spike rather than a continuous distribution, such as an exponential with scale parameter much smaller than  $\tau_i^2 \sigma^2$ . This allows for  $\beta_i$  to be sampled as identically zero, rather than a very small value. Furthermore, it eliminates the need to prescribe or infer the scale parameter of the narrow distribution approximating the discrete point-mass, which can be challenging to do in such a way that the MCMC sampler is efficient and mixes well.

### 3.1.3 Parameter layer

The remaining model parameters are given the following priors:

$$\theta_i \sim \text{Beta}(a_i, b_i)$$

$$\tau_i^2 \sim \text{Inv-Gamma}(c_i, d_i)$$

$$\sigma^2 \sim \text{Inv-Gamma}(\nu/2, \nu/2)$$

$$\nu \sim \text{Inv-Gamma}(\alpha_1, \alpha_2)$$

$$r \sim \text{Uniform}(0, 1).$$

Fixed hyperparameters  $a_i$ ,  $b_i$ ,  $c_i$ , and  $d_i$  control our prior belief about the probability that  $\beta_i$  is non-zero and about the scale of  $\beta_i$ . For example, heaters on oil and gas sites are not used in the summer, and as such the  $a_i$  and  $b_i$  hyperparameters could be set such that  $\theta_i$  has more mass close to zero in the prior during these months. By default, however, we use a uniform prior for  $\theta_i$  by setting  $a_i = b_i = 1$  and relatively uninformative priors for the remaining parameters by setting  $c_i = d_i = \alpha_1 = \alpha_2 = 1$ . The prior for  $\sigma^2$  was set such that, in the prior model, the  $\epsilon$  are distributed according to a Student's t-distribution with  $\nu$  degrees of freedom, as we discovered that the  $\epsilon$  can be heavier tailed than a Gaussian through basic model diagnostics.

## 3.2 Posterior inference

For methane emission source apportionment on oil and gas sites, the joint posterior distribution for the emission rates,  $\beta$ , and the indicator variables,  $z$ , are the most useful model output. If we let  $\xi$  be a vector of all model parameters,  $\xi = \{\beta_1, \dots, \beta_p, z_1, \dots, z_p, \theta_1, \dots, \theta_p, \tau_1^2, \dots, \tau_p^2, \sigma^2, \nu, r\}$ , then Bayes' theorem gives us the full joint distribution:  $p(\xi|\mathbf{y}) \propto p(\mathbf{y}|\xi)p(\xi)$ , where  $p(\cdot)$  denotes a probability density. We obtain samples from the joint posterior using a Markov chain Monte Carlo (MCMC) algorithm. We describe our MCMC algorithm below, but see Gelman et al. (2015) for a more complete discussion of Bayesian inference via MCMC.

We sample from the joint posterior using a Metropolis-within-Gibbs algorithm. We are able to derive a closed form expression for the conditional distributions of all model parameters except  $\nu$  and  $r$ , resulting in a fast sampler that mixes well. For  $\nu$  and  $r$ , we update using two Metropolis-Hastings steps within the Gibbs sampler that use a Gaussian as the candidate distribution. We use the posterior mean of the MCMC samples as a point estimate of emission rate in all subsequent analysis. Section S3 in the SI contains a derivation of each conditional distribution used in the sampler.

## 3.3 Inference on a moving time window

The MDLQ model assumes that emission rates are constant over the timeframe of the inversion, but methane emissions on oil and gas sites are highly variable over time. We therefore propose a windowed analysis when using the MDLQ in practice. Specifically, we propose running the MDLQ model on a 30-minute inversion window that is moved forward in 10-minute increments as new data are collected. Running the MDLQ model on a shorter window would be more likely to satisfy the constant emission source assumption, but would result in higher variability in the inferred emission characteristics given the smaller sample

Table 1: Information content of the CMS data across the METEC experiment.

<b>Number of sources with downwind sensors</b>	5	4	3	2	1	0
<b>Percent of inversion windows</b>	69.4%	17.5%	8.7%	3.9%	0.2%	0.2%

size. We find that a 30-minute inversion length provides a compromise between these two competing effects, and we present a sensitivity study of this length in Section S4 of the SI.

### 3.4 Assessing the information content of each inversion window

Occasionally, there are no CMS sensors downwind of one or more sources for an entire 30-minute inversion window. When this happens, the sensors will not detect elevated concentration values if one of these sources is emitting, and as such, they provide no information about the emission state of these sources. We therefore avoid making inference on sources with no downwind sensors during a given inversion window. We can identify these sources before running the inversion via the design matrix,  $X$ ; columns of  $X$  that consist of only zero concentration predictions likely have no downwind sensor during that inversion window. In this study, we say that the “viable sources” for a given window are those whose columns of  $X$  contain at least four non-zero concentration predictions. For each window, we subset  $X$  to just the viable sources and run the inversion as described in Section 3.2, resulting in a rate estimate for only the viable sources. The percent of inversion windows with information on each subset of sources is given in Table 1.

We note that  $\mathbf{y}$  will be identically  $\mathbf{0}$  for some inversion windows (e.g., from 4:00 and 8:00 in Figure 2). This corresponds to periods where the CMS sensors did not detect methane concentrations above background levels. When this occurs, we set the emission rate for all viable sources to 0 kg/hr without running the MDLQ model. As discussed above, we



make no inference on sources with no downwind sensors, and as such, we do not set their emission rate to zero in this situation.

### 3.5 Emissions inventories and alerts

Emission mitigation using CMS is done through two primary mechanisms: emissions inventories and alerts. Here we define these two terms and describe how output from the MDLQ model can be used to create inventories and alerts to drive emission reduction.

A source-level inventory estimates how much methane a given source emitted over a certain period of time (here we use the length of the METEC study). Accurate inventories are necessary to implement regulatory penalties for excess emissions and to ensure that long term emission reduction strategies are working. We create source-level inventories by multiplying the posterior mean of  $\beta$  for each inversion window by the length of the window and then summing across the duration of the experiment (averaging the temporal domain where windows overlap). We create 95% confidence intervals on the source-level inventories by sampling from the posterior distribution of  $\beta$  for each interval, creating source-level inventories for each sample, and then selecting the 0.025<sup>th</sup> and 0.975<sup>th</sup> percentiles of the resulting inventory distributions. We create a site-level inventory by summing the source-level inventories. When a source has no emission rate for a given inversion window due to a lack of information (i.e., no downwind sensor), we sample from the other rate estimates for that source when calculating the inventory. This procedure is justified because there is low correlation between emission characteristics (e.g., rate) and wind direction, which determines when there are downwind sensors of the potential sources.

An emission alert contains a point estimate of which equipment are emitting at the time of the alert. Oil and gas operators use alerts to determine whether detected emissions are

from normally operating equipment or from malfunctioning equipment that require immediate intervention. The proportion of posterior samples where  $z_i = 1$  gives the probability that source  $i$  is emitting. We therefore create a point estimate of the emission state of source  $i$  for a given inversion window as follows. If the posterior mean of  $z_i$  is greater than the average of  $z_i$  across all other windows, then we say that source  $i$  is emitting during that inversion window. We do not create alerts when the CMS data do not contain information for a given source.

## 4 Results

### 4.1 Methane emission source apportionment at METEC

We begin by showing output from the MDLQ model over an example 5-day period in Figure 5. We make two observations. First, the MDLQ model successfully distinguishes periods of emissions from periods of no emissions; it rarely infers a non-zero emission rate when no controlled releases are occurring. Second, inferred emission rates vary over the course of each release, despite the true emission rates being constant. This is because the 30-minute inversion windows are shorter than most releases, and inadequacies of the GPM will cause individual inversion windows to either over or underestimate the true emission rate.

We now summarize our source apportionment results over the entire METEC experiment, focusing on the MDLQ model’s ability to produce inventories and alerts. Figure 6(a) shows site- and source-level inventories for the study period. The site-level inventory is extremely close to truth, underestimating by only 1.0%. This is promising, as site-level inventories are the primary tool for emissions accounting in US regulations (EPA 2024), EU import standards (Council of European Union 2023), and voluntary emission management

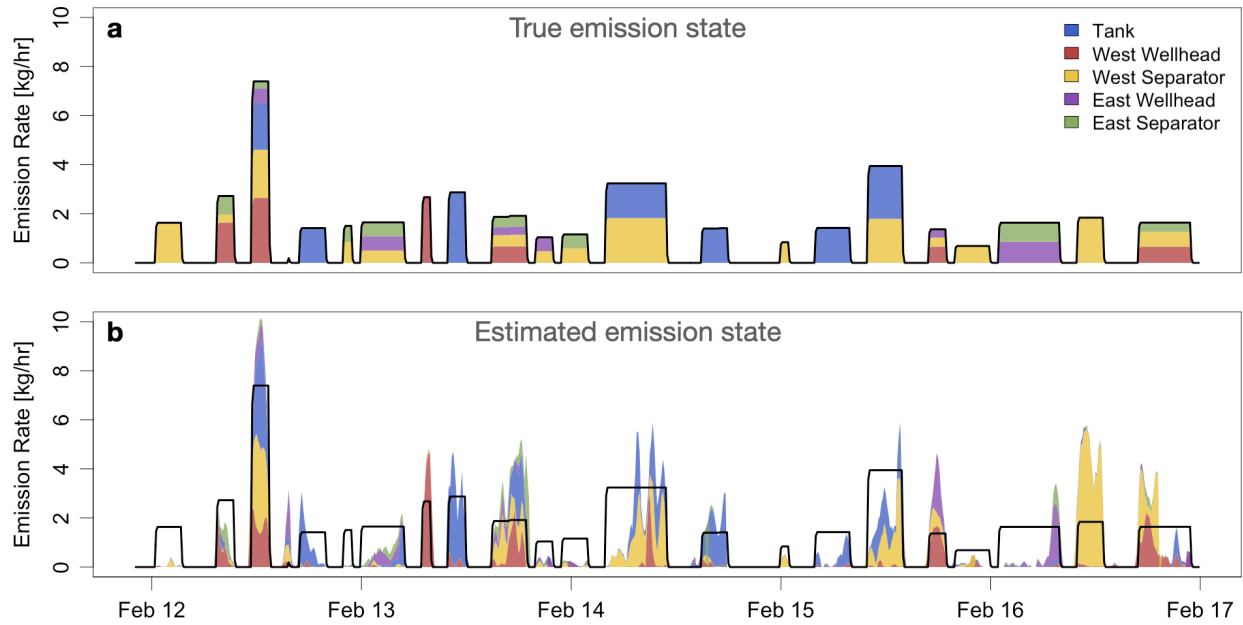


Figure 5: Output from the MDLQ model during 5 days of the METEC controlled releases. (a) shows the true emission state and (b) shows the estimated emission state from the MDLQ model. Color corresponds to the emitting equipment, and the black line shows the true site-level total emission rate over time.

protocols (OGMP 2.0 2024). However, the tank inventory is overestimated by 61.4% and the east separator inventory is underestimated by -38.8%. The remaining source-level inventories are slightly underestimated with errors ranging from -3.7% to -26.3%. The cause of these source-level inventory errors is investigated fully in Section S5 of the SI, but, in short, they are likely a result of inversion windows with downwind sensors for only a subset of the window. When there is no downwind sensor for the entire window, the MDLQ model does not infer an emission rate (as discussed in Section 3.4). However, when only a subset of the window has a downwind sensor, it naively appears as if no emissions occurred during the remainder of the window and an emission rate is still inferred. This happens more often for the sources that are close to the perimeter of the site and less often for the tanks, which are centrally located. As a result of this geometry, the MDLQ model likely overestimates tank emissions to compensate for the missed emissions from the remaining sources. To test this, we keep only the inversion windows that have downwind sensors for the entire window

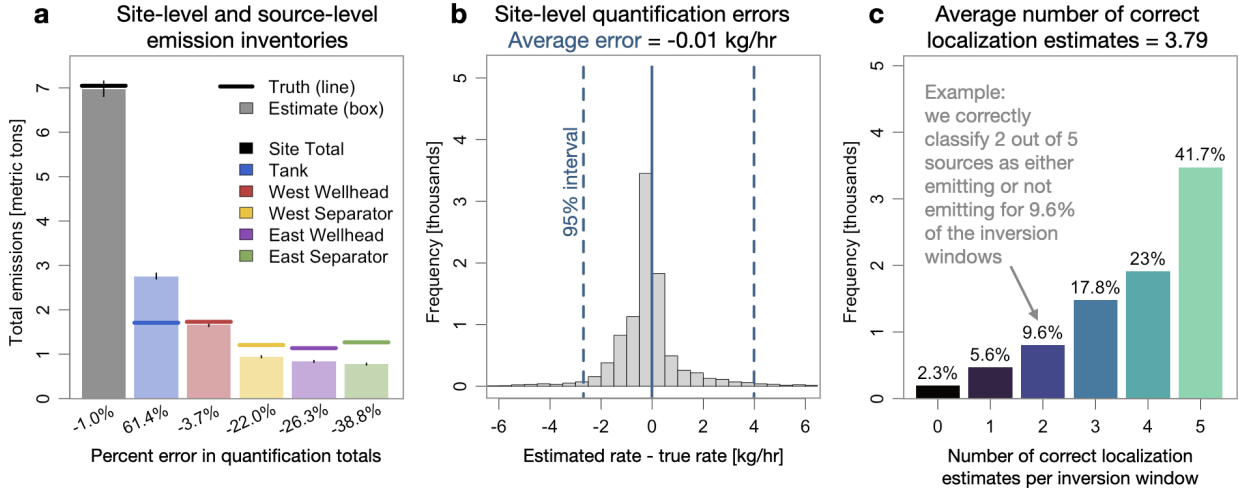


Figure 6: *Summary of the source apportionment results for the METEC controlled releases. (a) Site- and source-level inventories created by summing the emission rate estimates across all inversion windows. Vertical lines show 95% confidence intervals. (b) Distribution of errors in the site-level emission rate estimates. (c) Alerting accuracy, where a correct localization estimate is a correct estimate of emission state (i.e., either emitting or not emitting).*

and re-calculate the inventories. The resulting site-level inventory remains accurate (error = 1.7%) and the accuracy of the source-level inventories are much improved, with errors ranging from -23.4% to 24.2% (much closer to the inventories' confidence intervals). This filtering, however, significantly reduces the amount of data available to apportion emissions.

Figure 6(b) shows the distribution of errors in the site-level emission rate estimates across all inversion windows. The average error is -0.01 kg/hr, which makes sense given the small error in the site-level inventory from Figure 6(a). However, the inner 95% interval of the site-level errors is [-2.7, 4.0] kg/hr, meaning that there is relatively large variability in the individual site-level rate estimates. We also observed this fact in the example in Figure 5. This finding gives rise to the question: how many emission rate estimates need to be averaged before the site-level estimate is close to the truth? We investigate this question in Section S6 of the SI, and find that there is a 95% chance that the site-level error is within [-1, 1] kg/hr after averaging just 21 inversion windows (or approximately 11 hours). The fast convergence of the average is because there is low bias in the site-level rate estimates.

Table 2: Source- and site-level detection metrics for the METEC experiment. TPR = true positive rate, TNR = true negative rate, PPV = positive predictive value, and NPV = negative predictive value.

	<b>West Wellhead</b>	<b>West Separator</b>	<b>Tanks</b>	<b>East Wellhead</b>	<b>East Separator</b>	<b>Site- level</b>
<b>TPR</b>	67.6%	53.9%	59.2%	64.1%	60.7%	82.7%
<b>TNR</b>	81.5%	80.1%	72.3%	84.1%	84.2%	76.3%
<b>PPV</b>	56.1%	53.3%	46.3%	60.1%	63.9%	84.8%
<b>NPV</b>	87.8%	80.5%	81.5%	86.3%	82.3%	73.4%
<b>Accuracy</b>	77.9%	72.4%	68.5%	78.7%	76.8%	80.2%

Although this fact is not shown in Figure 6(b), we note that the coverage of the 95% credible intervals for the site-level rate estimates is only 0.58, meaning that we have missed a source of uncertainty in the MDLQ model. The missing uncertainty is very likely coming from bias in the GPM, as this model (while more accurate than comparable dispersion models) is still an oversimplification of actual atmospheric transport. We test this theory via a simulation study discussed shortly in Section 4.2.

Figure 6(c) assesses the accuracy of the alerts generated by the MDLQ model. For each inversion window, we check if the localization estimate (i.e., the emission state estimate) for each source is correct. That number, ranging from 0 to 5, is plotted in Figure 6 for all inversion windows. On average, the MDLQ correctly identifies 3.79 out of the 5 possible source as either emitting or not emitting. It most frequently identifies all 5 sources correctly, doing so for 41.7% of the windows. Table 2 shows additional detection metrics at both the source- and site-level. The MDLQ model detects 82.7% of emissions at the site-level, but is only able to detect 53.9% to 67.6% of emissions at the source-level. In other words, if a piece of equipment is leaking on the site, the MDLQ model will likely detect it and can generate an alert for the site. However, determining exactly which subset of sources is emitting is a harder problem, and the MDLQ model is more prone to errors in this use case. Full source- and site-level confusion matrices are provided in Section S7 of the SI.

## 4.2 Simulation study

We conduct a simulation study to isolate the effect of known biases in the GPM from other potential sources of error. Specifically, we study the impact of misaligned enhancements between the GPM predictions and CMS sensor observations, examples of which can be seen in Figure 3. This behavior is a result of various inadequacies of the GPM, such as not resolving turbulent eddy motion or obstructions.

We design the simulation study using the same physical geometry (i.e., source and sensor locations), wind data, and emission characteristics (i.e., timing and rate) as the METEC experiment. For each 30-minute inversion window, we construct the artificial observations as

$$\tilde{\mathbf{y}} = X\boldsymbol{\beta}_T + \tilde{\boldsymbol{\epsilon}},$$

where  $\boldsymbol{\beta}_T$  are the true emission rates,  $X$  is the GPM output (as defined in Section 3), and  $\tilde{\boldsymbol{\epsilon}} \sim N(0,1)$ . This setup eliminates forward model errors from  $\tilde{\mathbf{y}}$ , allowing us to reintroduce them in a controlled manner to gauge their impact on the MDLQ output. We reintroduce GPM bias by first identifying groups of concentration enhancements in  $\tilde{\mathbf{y}}$  using the gradient-based spike detection algorithm from Daniels et al. (2024a). We then move  $M$  percent of the enhancements to a different (uniformly sampled) time during the inversion window. For this study, we test five different values for  $M$ :  $\{0, 12.5, 25, 37.5, 50\}$ . We selected a maximum misalignment of 50% by examining real model-data mismatch during the METEC experiment; the percent of misaligned concentration enhancements rarely exceeded 50%. After introducing the artificial GPM bias, we run the MDLQ as described in Section 3.3 using  $\tilde{\mathbf{y}}$  instead of the actual CMS observations.

Figure 7 shows the results of this simulation study. We plot four response features for each value of  $M$ : the error variance, the autocorrelation coefficient, error in the emission

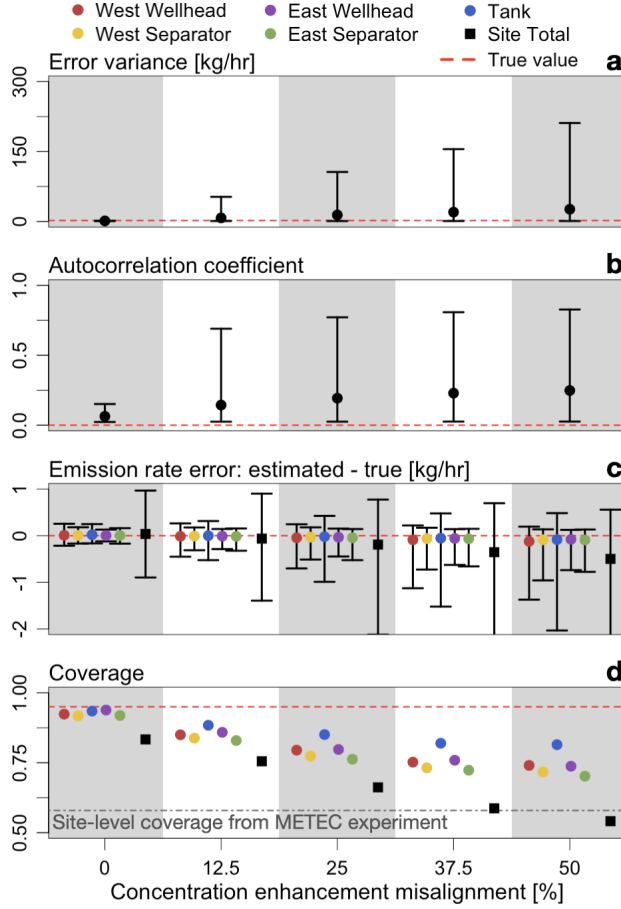


Figure 7: *Simulation study showing MDLQ performance under different levels of forward model bias. Red horizontal lines show the true values for each response feature. Bars show the inner 95% range for each value across the inversion windows. Colored circles correspond source-level results, and black squares correspond to site-level results.*

rate estimates, and the coverage of the emission rate credible intervals. In subfigures (a)-(c), we plot the mean of each response feature across all inversion windows, with black bars showing their inner 95% range. In subfigures (c)-(d), we show results separated by emission source (in color) and when summed to the site total (in black). For subfigure (d), coverage is computed as the percent of inversion windows where the true emission rate was contained within the corresponding 95% credible interval.

We make three observations. First, all parameters are successfully estimated in the absence of forward model bias, as expected, with source-level coverages close to 95%. The site-level coverage is lower than 95% because the site-level credible interval will not contain

the truth when any of the source-level credible intervals do not contain the truth. Since errors in the source-level rate estimates do not always occur during the same inversion window, the site-level credible interval will contain the truth for less than the expected 95% of inversion windows. Second, we see a diminishing ability to estimate  $\sigma^2$  and  $r$  as the degree of forward model bias increases, but emission rate estimates remain largely unbiased with a slight tendency to underestimate. This is promising, as  $\beta$  are the parameters of direct interest for methane emission source apportionment. The overestimation of  $\sigma^2$  is because the misaligned concentration enhancements result in extremely large errors, either positive or negative, which the Gaussian error model is not flexible enough to accommodate. Some of these errors are likely misinterpreted as autocorrelation, resulting in overestimates of  $r$ . Finally, source and site-level coverages drop as the degree of forward model bias increases and align with the coverage values seen during the METEC experiment. A drop in coverage is expected, as the misaligned enhancements result in either over or underestimation of  $\beta$ , such that many of the 95% credible intervals (which are not aware of the GPM bias) no longer contain the truth. Site-level coverage for the METEC experiment was 0.58, and source-level coverages ranged from 0.68 to 0.76. These values align closely with the coverages seen in the simulation study, providing evidence that GPM bias is indeed the cause of the coverage issues during the METEC controlled releases.

Section S8 in the SI contains an additional simulation study demonstrating the importance of modeling autocorrelation in  $\epsilon$ ; failing to do so results in overestimated  $\beta$  and low coverages.



### 4.3 Comparison to alternative methods

We analyze the METEC experiment using two basic statistical techniques (OLS and LASSO) and three state-of-the-art inversion methods from the literature, with results summarized in Table 3. We select two single-source methods to compare against (Cartwright et al. 2019, Daniels et al. 2024a), both of which assume that only one source is emitting at a time. To apply them to the METEC data, we use the localization procedure from Daniels et al. (2024a) to estimate a most likely source for each inversion window before the inversion is performed. We select one multisource method to compare against (Weidmann et al. 2022), which can either estimate fluxes on a fixed grid or identify emitting sources using a reversible jump MCMC sampler. To provide a fair comparison, we use this method with a fixed grid that is constrained to the locations of the five sources on the METEC site, as the MDLQ model specifies these sources a priori. Finally, we also compare to a variant of the MDLQ model that assumes independent Laplace errors. Through basic model diagnostics, we found that errors from the MDLQ model often have heavier tails than a Gaussian. These large errors are likely from instances in which a spike in the concentration predictions is not present in the observations, or visa versa. We believed that a Laplace error model might be better able to capture large errors and hence result in better coverage. Section S9 of the SI fully defines this model variant. As none of these alternative methods discuss how to best use their inversion method in practice (rather than on releases with known start and end times), we use the moving time window approach discussed in Section 3.3 for all methods.

Table 3: Comparison to alternative methods using data from the METEC controlled releases. Site-level total error is the error (estimate - truth) in the site-level inventory. The following five rows provide the source-level inventory errors (estimate - truth). Errors are presented in units of metric tons (t) and as percent errors. Average site-level quantification error is the average error (estimate - truth) across all individual site-level emission rate estimates, and the IQR of these errors is the difference between their 25th and 75th percentiles. Coverage of the site-level 95% credible intervals is the fraction of inversion windows where the true site-level emission rate was contained within the 95% credible interval of the estimate. The average number of correct localization estimates is the average number of correct state estimates (either on or off) across all inversion windows.

	Basic statistical methods		Single-source methods		Multisource methods		
	OLS	LASSO	Daniels et al. (2024)	Cartwright et al. (2019)	Weidmann et al. (2022)	MDLQ Laplace errors	MDLQ
Site-level total error	4.4 t (62.3%)	1.5 t (20.7%)	0.3 t (4.6%)	4.2 t (59.7%)	-0.8 t (-11.9%)	4.7 t (66.4%)	<b>-0.1 t</b> <b>(-1.0%)</b>
West wellhead total error	0.8 t (46.0%)	0.01 t (0.7%)	0.3 t (19.7%)	<b>0.003 t</b> <b>(0.2%)</b>	-0.5 t (-29.4%)	0.6 t (32.0%)	-0.1 t (-3.7%)
West separator total error	0.2 t (14.5%)	-0.1 t (-10.9%)	-0.2 t (-13.0%)	<b>0.1 t</b> <b>(7.3%)</b>	-0.2 t (-17.4%)	0.7 t (55.2%)	-0.3 t (-22.0%)
Tank total error	2.6 t (153.4%)	1.6 t (95.4%)	0.9 t (52.4%)	0.8 t (44.9%)	<b>0.2 t</b> <b>(13.8%)</b>	1.3 t (78.9%)	1.0 t (61.4%)
East wellhead total error	0.7 t (60.5%)	0.2 t (16.6%)	-0.2 t (-18.5%)	1.9 t (171.0%)	<b>-0.1 t</b> <b>(-11.8%)</b>	1.0 t (83.8%)	-0.3 (-26.3%)
East separator total error	<b>0.1 t</b> <b>(8.7%)</b>	-0.2 t (-18.6%)	-0.5 t (-42.9%)	1.4 t (111.1%)	-0.2 t (-17.7%)	1.2 t (91.5%)	-0.5 t (-38.8%)
Avg site-level quant error	0.61 kg/hr	0.24 kg/hr	0.08 kg/hr	0.70 kg/hr	-0.25 kg/hr	0.82 kg/hr	<b>-0.01</b> <b>kg/hr</b>
IQR of site-level quant errors	0.75 kg/hr	0.66 kg/hr	0.74 kg/hr	3.72 kg/hr	<b>0.62</b> <b>kg/hr</b>	0.67 kg/hr	0.76 kg/hr
Site-level coverage of 95% CI	N/A	N/A	<b>0.66</b>	0.40	0.33	0.51	0.58
Avg number of correct localization estimates	4.15 out of 5	4.09 out of 5	3.96 out of 5	3.57 out of 5	4.02 out of 5	<b>4.16</b> <b>out of</b> <b>5</b>	3.79 out of 5

The MDLQ model has the smallest error in the site-level inventory and in the individual site-level emission rate estimates. No one method has the smallest error across the five source-level inventories. Weidmann et al. (2022) provides the best Tank and East Wellhead inventory, Cartwright et al. (2019) provides the best West Wellhead and West Separator inventory, and OLS provides the best East Separator inventory. Weidmann et al. (2022) has the smallest IQR. The single-source inversion method from Daniels et al. (2024a) has the best coverage, followed by the MDLQ. The MDLQ model variant with Laplace errors has the best localization performance, closely followed by OLS. Note that for OLS, LASSO, and the method from Weidmann et al. (2022), we assume that a source is emitting if its rate estimate is above 0.1 kg/hr, which was hand-tuned to provide the best possible localization performance on these data.

## 5 Discussion

We have proposed a Bayesian hierarchical model for methane emission source apportionment on oil and gas sites, referred to as the MDLQ model. This model is able to estimate total emissions on a representative oil and gas site to within 0.1 metric tons over the course of a three month experiment, a percent error of just -1.0%.

The primary statistical contribution of this work is the synthesis and extension of other source apportionment methods from the existing literature, such as the spike-and-slab prior from Weidmann et al. (2022), the autocorrelated error model from Ganesan et al. (2014), and the time-varying Gaussian puff atmospheric dispersion model from Jia et al. (2025). We extend these studies and synthesize their contributions in the MDLQ model. Our implementation of the model is able to achieve a 100% convergence rate due to several innovative steps of the Gibbs sampler that are described fully in Section S3 of the SI.

The primary contribution of this work to the field of methane emissions mitigation is twofold. First, we provide the most accurate CMS-based inversion method for creating site-level emissions inventories to date. Site-level inventories are an important tool for emissions accounting and mitigation in US regulations (EPA 2024), EU import standards (Council of European Union 2023), and voluntary emission management protocols (OGMP 2.0 2024). The inversion performance of many commercially available CMS solutions is lacking (Ilonze et al. 2024, Chen et al. 2024, Daniels et al. 2025), and we hope to elevate all solutions operating in this space by making the MDLQ model implementation fully open source. Second, the METEC experiment provides a more robust evaluation of source apportionment methods for oil and gas sites than other experiments in the literature, as it contains about 10 times more releases and uses more realistic emission characteristics. As such, we believe that the results in this paper are more likely to generalize to real oil and gas sites, and by making all data from this study open source, we hope to provide a robust test bed for future modeling efforts.

We conclude by discussing two limitations of the MDLQ model and future lines of research that may address them. First, the MDLQ model does not learn any parameters of the forward atmospheric dispersion model as is done in Cartwright et al. (2019) or Newman et al. (2024) and instead prescribes them based on atmospheric stability class. This may contribute to the large variability in inferred emission rates, as the Pasquill-Gifford-Turner dispersion scheme can overestimate or underestimate true atmospheric dispersion. Developing a faster implementation of the Gaussian puff model (or another fast solution to the advection-diffusion equation) may make it feasible to sample dispersion parameters within the MCMC without having to use the lower fidelity Gaussian plume model (Jia et al. 2025). Second, errors in the source-level inventories range from -38.8% to 61.4% when using all

available data, but are significantly reduced when using just the inversion windows that have at least one sensor downwind of all sources for the entire window. With this in mind, we will investigate an adaptive windowing approach where the exact boundaries of each inversion window are based on the information content of the CMS data rather than being fixed at 30-minute intervals. Additionally, using a probabilistic sampling scheme similar to the one proposed in Daniels et al. (2024b) may provide a better way to extrapolate emission rate estimates from windows with full information to the desired temporal range (e.g., an annual inventory for regulatory reporting). We believe that these efforts would improve source-level inventories and alerts derived from the MDLQ model.

## Code and data availability

All code and data required to reproduce the results in this manuscript will be made open source upon publication. Anonymized code and data will be made available to referees during the review process.

## References

- Ars, S., Broquet, G., Yver Kwok, C., Roustan, Y., Wu, L., Arzoumanian, E. & Bousquet, P. (2017), ‘Statistical atmospheric inversion of local gas emissions by coupling the tracer release technique and local-scale transport modelling: a test case with controlled methane emissions’, *Atmospheric Measurement Techniques* **10**(12), 5017–5037. <https://doi.org/10.5194/amt-10-5017-2017>.
- Bodin, T., Sambridge, M., Gallagher, K. & Rawlinson, N. (2012), ‘Transdimensional inver-

- sion of receiver functions and surface wave dispersion’, *Journal of Geophysical Research: Solid Earth* **117**(B2). <https://doi.org/10.1029/2011JB008560>.
- Cartwright, L., Zammit-Mangion, A., Bhatia, S., Schroder, I., Phillips, F., Coates, T., Negandhi, K., Naylor, T., Kennedy, M., Zegelin, S., Wokker, N., Deutscher, N. M. & Feitz, A. (2019), ‘Bayesian atmospheric tomography for detection and quantification of methane emissions: application to data from the 2015 Ginninderra release experiment’, *Atmospheric Measurement Techniques* **12**(9), 4659–4676. <https://doi.org/10.5194/amt-12-4659-2019>.
- Chen, Z., El Abbadi, S. H., Sherwin, E. D., Burdeau, P. M., Rutherford, J. S., Chen, Y., Zhang, Z. & Brandt, A. R. (2024), ‘Comparing Continuous Methane Monitoring Technologies for High-Volume Emissions: A Single-Blind Controlled Release Study’, *ACS ES&T Air* **1**(8), 871–884. <https://doi.org/10.1021/acsestair.4c00015>.
- Council of European Union (2023), ‘Council regulation (EU) 2019/942 (COM(2021)0805 – C9-0467/2021 – 2021/0423(COD))’. [https://www.europarl.europa.eu/doceo/document/TA-9-2023-0127\\_EN.html](https://www.europarl.europa.eu/doceo/document/TA-9-2023-0127_EN.html).
- Crippa, M., Guizzardi, D., Muntean, M., Schaaf, E., Lo Vullo, E., Solazzo, E., Monforti-Ferrario, F., Olivier, J. & Vignati, E. (2021), ‘EDGAR v6.0 Greenhouse Gas Emissions’. <http://data.europa.eu/89h/97a67d67-c62e-4826-b873-9d972c4f670b>.
- Cusworth, D. H., Duren, R. M., Thorpe, A. K., Olson-Duvall, W., Heckler, J., Chapman, J. W., Eastwood, M. L., Helmlinger, M. C., Green, R. O., Asner, G. P., Dennison, P. E. & Miller, C. E. (2021), ‘Intermittency of Large Methane Emitters in the Permian Basin’, *Environmental Science & Technology Letters* **8**(7), 567–573. <https://doi.org/10.1021/acs.estlett.1c00173>.

- Daniels, W. S., Jia, M. & Hammerling, D. M. (2024a), ‘Detection, localization, and quantification of single-source methane emissions on oil and gas production sites using point-in-space continuous monitoring systems’, *Elementa: Science of the Anthropocene* **12**(1), 00110. <https://doi.org/10.1525/elementa.2023.00110>.
- Daniels, W. S., Jia, M. & Hammerling, D. M. (2024b), ‘Estimating Methane Emission Durations Using Continuous Monitoring Systems’, *Environmental Science & Technology Letters* **11**(11), 1187–1192. <https://doi.org/10.1021/acs.estlett.4c00687>.
- Daniels, W. S., Kidd, S. G., Yang, S. L., Stokes, S., Ravikumar, A. P. & Hammerling, D. M. (2025), ‘Intercomparison of Three Continuous Monitoring Systems on Operating Oil and Gas Sites’, *ACS ES&T Air* **2**(4), 564–577. <https://doi.org/10.1021/acsestair.4c00298>.
- Daniels, W. S., Wang, J. L., Ravikumar, A. P., Harrison, M., Roman-White, S. A., George, F. C. & Hammerling, D. M. (2023), ‘Toward Multiscale Measurement-Informed Methane Inventories: Reconciling Bottom-Up Site-Level Inventories with Top-Down Measurements Using Continuous Monitoring Systems’, *Environmental Science & Technology* **57**(32), 11823–11833. <https://doi.org/10.1021/acs.est.3c01121>.
- EPA (1992), Workbook for plume visual impact screening and analysis (revised), Technical Report 450-4-88-015, U.S. Environmental Protection Agency.
- EPA (2024), Greenhouse Gas Reporting Rule: Revisions and Confidentiality Determinations for Petroleum and Natural Gas Systems, Final Rule 89 FR 42062, U.S. Environmental Protection Agency. <https://www.federalregister.gov/d/2024-08988>.
- Ganesan, A. L., Rigby, M., Zammit-Mangion, A., Manning, A. J., Prinn, R. G., Fraser, P. J., Harth, C. M., Kim, K.-R., Krummel, P. B., Li, S., Mühle, J., O’Doherty, S. J.,

- Park, S., Salameh, P. K., Steele, L. P. & Weiss, R. F. (2014), ‘Characterization of uncertainties in atmospheric trace gas inversions using hierarchical Bayesian methods’, *Atmospheric Chemistry and Physics* **14**(8), 3855–3864. <https://doi.org/10.5194/acp-14-3855-2014>.
- Gelman, A., Carlin, J. B., Stern, H. S., Dunson, D. B., Vehtari, A. & Rubin, D. B. (2015), *Bayesian Data Analysis*, 3 edn, Chapman and Hall/CRC, New York. <https://doi.org/10.1201/b16018>.
- Hirst, B., Randell, D., Jones, M., Chu, J., Kannath, A., Macleod, N., Dean, M. & Weidmann, D. (2020), ‘Methane Emissions: Remote Mapping and Source Quantification Using an Open-Path Laser Dispersion Spectrometer’, *Geophysical Research Letters* **47**(10), e2019GL086725. <https://doi.org/10.1029/2019GL086725>.
- Ilonze, C., Emerson, E., Duggan, A. & Zimmerle, D. (2024), ‘Assessing the Progress of the Performance of Continuous Monitoring Solutions under a Single-Blind Controlled Testing Protocol’, *Environmental Science & Technology* **58**(25), 10941–10955. <https://doi.org/10.1021/acs.est.3c08511>.
- Jia, M., Fish, R., Daniels, W. S., Sprinkle, B. & Hammerling, D. (2025), ‘A fast and lightweight implementation of the Gaussian puff model for near-field atmospheric transport of trace gasses’, *Scientific Reports* **15**, 18710. <https://doi.org/10.1038/s41598-025-99491-x>.
- Kumar, P., Broquet, G., Caldow, C., Laurent, O., Gichuki, S., Cropley, F., Yver-Kwok, C., Fontanier, B., Lauvaux, T., Ramonet, M., Shah, A., Berthe, G., Martin, F., Duclaux, O., Juery, C., Bouchet, C., Pitt, J. & Ciais, P. (2022), ‘Near-field atmospheric inversions for the localization and quantification of controlled methane releases using station-



- ary and mobile measurements’, *Quarterly Journal of the Royal Meteorological Society* **148**(745), 1886–1912. <https://doi.org/10.1002/qj.4283>.
- Kunkel, W. M., Carre-Burritt, A. E., Aivazian, G. S., Snow, N. C., Harris, J. T., Mueller, T. S., Roos, P. A. & Thorpe, M. J. (2023), ‘Extension of Methane Emission Rate Distribution for Permian Basin Oil and Gas Production Infrastructure by Aerial LiDAR’, *Environmental Science & Technology* **57**(33), 12234–12241. <https://doi.org/10.1021/acs.est.3c00229>.
- Mitchell, T. J. & Beauchamp, J. J. (1988), ‘Bayesian Variable Selection in Linear Regression’, *Journal of the American Statistical Association* **83**(404), 1023–1032. <https://doi.org/10.1080/01621459.1988.10478694>.
- Newman, T., Nemeth, C., Jones, M. & Jonathan, P. (2024), ‘Probabilistic Inversion Modeling of Gas Emissions: A Gradient-Based MCMC Estimation of Gaussian Plume Parameters’. <https://doi.org/10.48550/arXiv.2408.01298>.
- Nisbet, E. G., Fisher, R. E., Lowry, D., France, J. L., Allen, G., Bakkaloglu, S., Broderick, T. J., Cain, M., Coleman, M., Fernandez, J., Forster, G., Griffiths, P. T., Iverach, C. P., Kelly, B. F. J., Manning, M. R., Nisbet-Jones, P. B. R., Pyle, J. A., Townsend-Small, A., al Shalaan, A., Warwick, N. & Zazzeri, G. (2020), ‘Methane Mitigation: Methods to Reduce Emissions, on the Path to the Paris Agreement’, *Reviews of Geophysics* **58**(1), e2019RG000675. <https://doi.org/10.1029/2019RG000675>.
- OGMP 2.0 (2024), ‘The Oil & Gas Methane Partnership 2.0’. UN Environment Programme (UNEP). <https://ogmpartnership.com/>.
- O’Rourke, P. R., Smith, S. J., Mott, A., Ahsan, H., McDuffie, E. E., Crippa, M., Klimont,

- Z., McDonald, B., Wang, S., Nicholson, M. B., Feng, L. & Hoesly, R. M. (2021), ‘CEDS v-2021-02-05 Emission Data 1975-2019’. <http://doi.org/10.5281/zenodo.4509372>.
- Pasquill, F. (1961), ‘The estimation of the dispersion of windborne material’, *Meteorological Magazine* **90**, 33–49.
- Stockie, J. M. (2011), ‘The Mathematics of Atmospheric Dispersion Modeling’, *SIAM Review* **53**(2), 349–372. <https://doi.org/10.1137/10080991X>.
- Szopa, S., Naik, V., Adhikary, B., Artaxo, P., Berntsen, T., Collins, W., Fuzzi, S., Gallardo, L., Kiendler-Scharr, A., Klimont, Z., Liao, H., Unger, N. & Zanis, P. (2021), ‘Short-Lived Climate Forcers’. In *Climate Change 2021: The Physical Science Basis. Contribution of Working Group I to the Sixth Assessment Report of the Intergovernmental Panel on Climate Change*. <https://doi.org/10.1017/9781009157896.008>.
- Turner, B. D. (1970), *Workbook of atmospheric dispersion estimates*, Technical Report 742-R-70-001, U.S. Environmental Protection Agency.
- Wang, J. L., Daniels, W. S., Hammerling, D. M., Harrison, M., Burmaster, K., George, F. C. & Ravikumar, A. P. (2022), ‘Multiscale Methane Measurements at Oil and Gas Facilities Reveal Necessary Frameworks for Improved Emissions Accounting’, *Environmental Science & Technology* **56**(20), 14743–14752. <https://doi.org/10.1021/ACS.EST.2C06211>.
- Weidmann, D., Hirst, B., Jones, M., Ijzermans, R., Randell, D., Macleod, N., Kannath, A., Chu, J. & Dean, M. (2022), ‘Locating and Quantifying Methane Emissions by Inverse Analysis of Path-Integrated Concentration Data Using a Markov-Chain Monte Carlo Approach’, *ACS Earth and Space Chemistry* **6**(9), 2190–2198. <https://doi.org/10.1021/acsearthspacechem.2c00093>.

World Economic Forum (2024), ‘Quantifying the Impact of Climate Change on Human Health’. <https://www.weforum.org/publications/quantifying-the-impact-of-climate-change-on-human-health/>.

Xue, F., Li, X., Ooka, R., Kikumoto, H. & Zhang, W. (2017), ‘Turbulent Schmidt number for source term estimation using Bayesian inference’, *Building and Environment* **125**, 414–422. <https://doi.org/10.1016/j.buildenv.2017.09.012>.